

The dark matter distribution in disk galaxies

Annamaria Borriello¹ & Paolo Salucci¹

(1) *International School of Advanced Studies SISSA-ISAS – Trieste, I*

31 October 2018

ABSTRACT

We use high-quality optical rotation curves of 9 low-luminosity disk galaxies to obtain the velocity profiles of the surrounding dark matter halos. We find that they increase linearly with radius at least out to the edge of the stellar disk, implying that, over the entire stellar region, the density of the dark halo is about constant.

The properties of the mass structure of these halos are similar to those found for a number of dwarf and low surface brightness galaxies, but provide a more substantial evidence of the discrepancy between the halo mass distribution predicted in the Cold Dark Matter scenario and those actually detected around galaxies. We find that the density law proposed by Burkert (1995) reproduces the halo rotation curves, with halo central densities ($\rho_0 \sim 1\text{--}4 \times 10^{-24} \text{ g cm}^{-3}$) and core radii ($r_0 \sim 5\text{--}15 \text{ kpc}$) scaling as $\rho_0 \propto r_0^{-2/3}$.

Key words: cosmology: dark matter – galaxies: spirals

1 INTRODUCTION

Rotation curves (RCs) of disk galaxies are the best probe for dark matter (DM) on galactic scale. Notwithstanding the impressive amount of knowledge gathered in the past 20 years, some crucial aspects of the mass *distribution* remain unclear. In fact, the actual density profile of dark halos is still matter of debate; we do not even know whether it is universal or related to some galaxy property, such as the total mass. This is partly because such issues are intrinsically crucial and partly because it is often believed that a RC leads to a quite ambiguous information on the dark halo density distribution (e.g. van Albada et al. 1985). However, this argument is true only for rotation curves of low spatial resolution, i.e. with no more than 2 measures per exponential disk length-scale R_D , as is the case of the great majority of HI RCs. This is because the galaxy structure parameters are very sensitive to both the *amplitude* and the *shape* of the rotation curve in the region $0 < r < R_D$, (e.g. Blais-Ouellette et al., 1999) which corresponds to the region of the RC steepest rise. No reliable mass model can be derived if such a region is poorly sampled and/or radio beam-biased. However, in case of high-quality *optical* RCs with tens of independent measurements in the critical region, the kinematics can probe the halo mass distribution and resolve their structure.

Since the dark component can be better traced when the disk contributes to the dynamics in a modest way, it is convenient to investigate DM-dominated objects, like dwarf and low surface brightness (LSB) galaxies. It is well known that for the latter there are strong claims of dark matter distributions with cores of constant density, in disagreement

Galaxy	R_D (kpc)	V_{opt} (km s ⁻¹)	M_I
116-G12	1.7	133.5	-20.0
531-G22	3.3	171.1	-21.4
533-G4	2.7	151.1	-20.7
545-G5	2.4	124.4	-20.4
563-G14	2.0	148.9	-20.5
79-G14	3.9	167.1	-21.4
M-3-1042	1.5	148.0	-20.1
N7339	1.5	172.7	-20.6
N755	1.5	102.4	-20.1

Table 1. Observational properties of the sample galaxies: (1) Galaxy name. (2) Length-scale of the exponential thin disk (from Persic & Salucci 1995). The optical radius R_{opt} is the radius encompassing 83% of the light: $R_{opt} = 3.2R_D$. (3) Circular velocity at R_{opt} . (4) Total *I*-band absolute magnitude (Mathewson, Ford & Buchhorn, 1992).

with the steeply cusped density distributions of the Cold Dark Matter Scenario. (Flores & Primack, 1994; Moore, 1994; Burkert, 1995; Burkert & Silk, 1997; Kravtsov et al., 1998; McGaugh & de Blok, 1998; Stil, 1999). However, these findings are 1) under the *caveat* that the low spatial resolution of the analysed RCs does not bias the mass modeling and 2) uncertain, due to the limited amount of available kinematical data (see van den Bosch et al., 1999).

In this paper we will investigate the above-discussed issue by analysing a number of high-quality *optical* rotation curves of *low luminosity* late-type spirals taken from

arXiv:astro-ph/0001082v2 12 Sep 2000

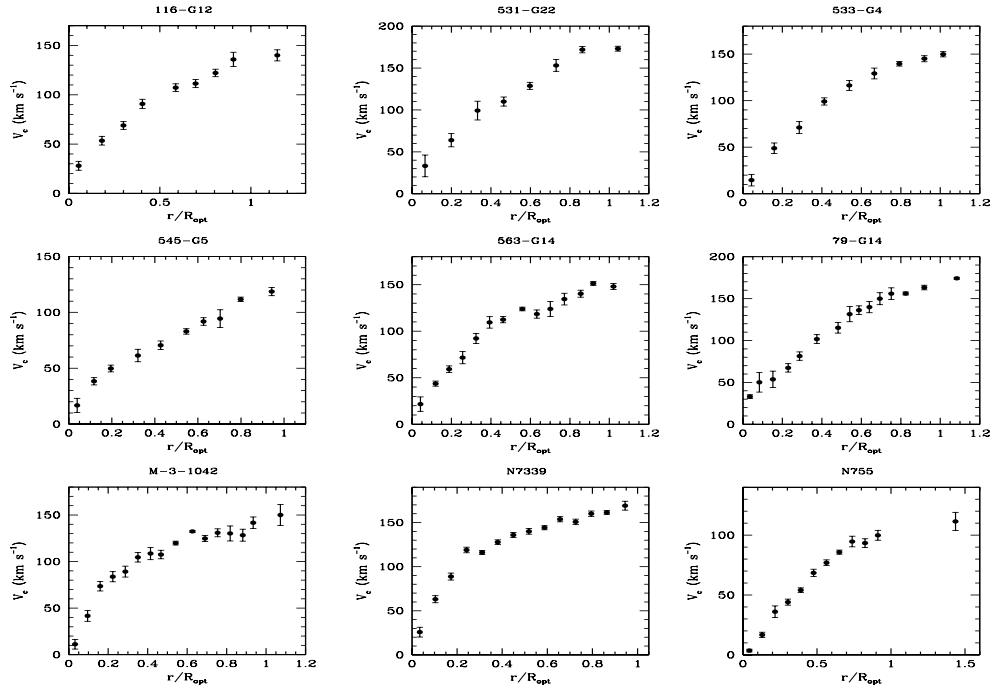


Figure 1. Rotation curves of the sample galaxies.

Persic and Salucci (1995, PS95), with I-band absolute magnitudes $-21.4 < M_I < -20.0$ that, in terms of rotational velocities, translates into $100 < V_{opt} < 170 \text{ km s}^{-1}$. Objects in this luminosity/velocity range are DM dominated (e.g. Persic, Salucci & Stel, 1996), but their RCs, measured at the PS95 angular resolution of $2''$, have a spatial resolution of $w \sim 100(D/10 \text{ Mpc}) \text{ pc}$ and $n_{data} \sim R_{opt}/w$ independent measurements. For nearby galaxies: $w \ll R_D$ and $n_{data} > 25$. Moreover, we select rotation curves of bulgeless systems, so that the stellar disk is the only baryonic component for $r \lesssim R_D$.

Since most of the properties of cosmological halos are claimed universal, it is worth to concentrate on a small and particular sample of RCs, that however can provide crucial information on the dark halo density distribution. The systematics and the cosmic variance of the DM halos are investigated elsewhere (Salucci and Burkert, 1999; Salucci, 1999). Finally, let us stress that to establish the *actual* theoretical properties of CDM halos or to investigate *non-standard* CDM scenarios possibly in agreement with observations is beyond the scope of this work.

In §2 we describe our sample of RCs. We present our mass modeling technique and its results in §3. In §4 we discuss the inferred halo profiles and their properties. In §5 we perform a disk-halo rotation curve modeling by adopting a CDM density profile for the dark halo. We summarize our results in §6. Throughout this paper we adopt a Hubble constant of $H_0 = 75 \text{ km s}^{-1} \text{ Mpc}^{-1}$.

2 ROTATION CURVES

The rotation curves of the Persic & Salucci (PS95) ‘excellent’ subsample of 80 galaxies are all suitable for an accurate mass modeling. In fact, these RCs properly trace the gravitational potential in that: 1) data extend at least to the optical radius, 2) they are smooth and symmetric, 3) they have small *rms*, 4) they have high spatial resolution and a homogeneous radial data coverage, i.e. about 30–100 data points homogeneously distributed with radius and between the two arms. From this subsample we extract 9 rotation curves of low luminosity galaxies ($5 \times 10^9 L_\odot < L_I < 2 \times 10^{10} L_\odot$; $100 < V_{opt} < 170 \text{ km s}^{-1}$), with their I-band surface luminosity being an (almost) perfect radial exponential. These two last criteria, not indispensable to perform the *mass* decomposition, are however required to minimize the uncertainties of the resulting dark halo *density* distribution. The selected RCs are shown in Figure 1 (for all details we refer to PS95). They are still growing at R_{opt} , in that mostly tracing the dark halo component. Each RC has 7–15 velocity points inside R_{opt} , each one being the average of 2–6 independent data. The RC spatial resolution is better than $1/20 R_{opt}$, the velocity *rms* is about 3% and the RCs logarithmic derivative is generally known within about 0.05.

3 MASS MODELING

We model the mass distribution as the sum of two components: a stellar disk and a spherical dark halo. By assuming

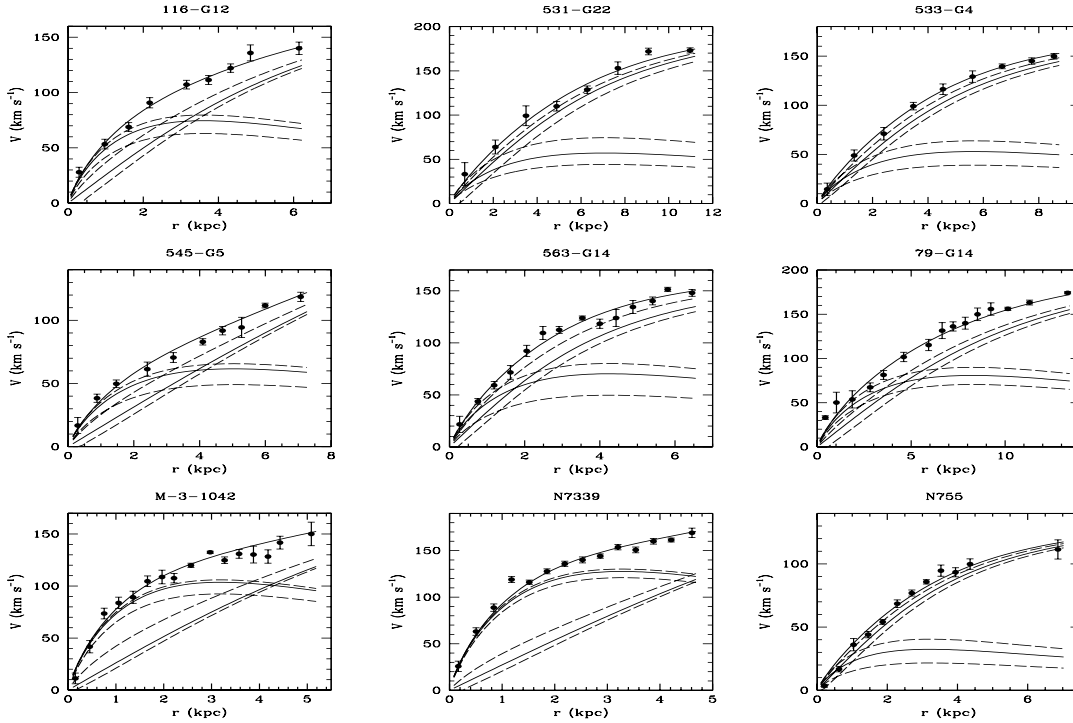


Figure 2. CDR model fits (*thick solid line*) to the RCs (*points with errorbars*). Thin solid lines represent the disk and halo contributions. The maximum disk and the minimum disk solutions are also plotted (*dashed lines*).

Galaxy	β	a	M_D/L_I
116-G12	$0.28^{+0.04}_{-0.08}$	$1.4^{+0.3}_{-0.2}$	$1.0^{+0.1}_{-0.3}$
531-G22	$0.10^{+0.07}_{-0.04}$	$0.8^{+0.8}_{-0.2}$	$0.3^{+0.2}_{-0.1}$
533-G4	$0.11^{+0.05}_{-0.05}$	$0.8^{+0.2}_{-0.1}$	$0.4^{+0.2}_{-0.2}$
545-G5	$0.22^{+0.03}_{-0.08}$	$2.5^{+0.5}_{-0.5}$	$0.7^{+0.1}_{-0.2}$
563-G14	$0.20^{+0.06}_{-0.10}$	$0.8^{+0.2}_{-0.2}$	$0.7^{+0.2}_{-0.3}$
79-G14	$0.21^{+0.05}_{-0.05}$	$1.0^{+0.1}_{-0.1}$	$0.7^{+0.2}_{-0.2}$
M-3-1042	$0.44^{+0.02}_{-0.09}$	$1.9^{+0.1}_{-1.1}$	$1.6^{+0.1}_{-0.3}$
N7339	$0.49^{+0.02}_{-0.05}$	$2.4^{+1.0}_{-0.7}$	$1.6^{+0.1}_{-0.2}$
N755	$0.09^{+0.05}_{-0.05}$	$1.0^{+0.1}_{-0.2}$	$0.2^{+0.1}_{-0.1}$

Table 2. CDR mass models: (1) Galaxy name; (2)-(3) Parameters of the best-fit CDR models with their 1σ uncertainties (§3); (4) Disk mass-to-light ratio in the I -band in solar units.

centrifugal equilibrium under the action of the gravitational potential, the observed circular velocity can be split into these two components:

$$V^2(r) = V_D^2(r) + V_H^2(r) \quad (1)$$

This is true as long as one assumes the galactic disk be in dynamic equilibrium. By selection, the objects are bulgeless and the stellar component is distributed like an exponen-

tial thin disk. Light traces the mass via an assumed radially constant mass-to-light ratio.

In the r.h.s of eq.(1) we neglect the gas contribution $V_{gas}(r)$ since in normal spirals it is usually modest within the optical region (Rhee (1996), Fig. 4.13): $\beta_{gas} \equiv (V_{gas}^2/V^2)_{R_{opt}} \sim 0.1$. Furthermore, high resolution HI observations show that in galaxies with RCs similar to those of the present sample (M33: Corbelli & Salucci, 1999; NGC300: Puche, Carignan & Bosma, 1990; N5585: Cote & Carignan, 1991; N3949 and N3917: Verheijen, 1997) $V_{gas}(r)$ is well represented by $V_{gas}(r) \simeq 0$ for $r < R_D$ and:

$$V_{gas}(r) \simeq (20 \pm 5)(r - R_D)/2R_D \quad R_D \leq r \leq 3R_D \quad (2)$$

Thus, in the optical region: *i*) $V_{gas}^2(r) \ll V^2(r)$ and *ii*) $d(V^2(r) - V_{gas}^2(r))/dr \gtrsim 0$. This last condition implies that by including V_{gas} in the r.h.s. of eq.(1) the halo velocity profiles would result *steeper* and then the core radius in the halo density *larger*. Incidentally, this is not the case for dwarfs and LSBs: most of their kinematics is affected by the HI disk gravitational pull in such a way that neglecting it could bias the determination of the DM density.

The circular velocity profile of the disk is (Freeman, 1970):

$$V_D^2(r) = V_{opt}^2 \beta \frac{r^2}{R_{opt}^2} \frac{(I_0 K_0 - I_1 K_1)_{1.6r/R_{opt}}}{(I_0 K_0 - I_1 K_1)_{1.6}} \quad (3)$$

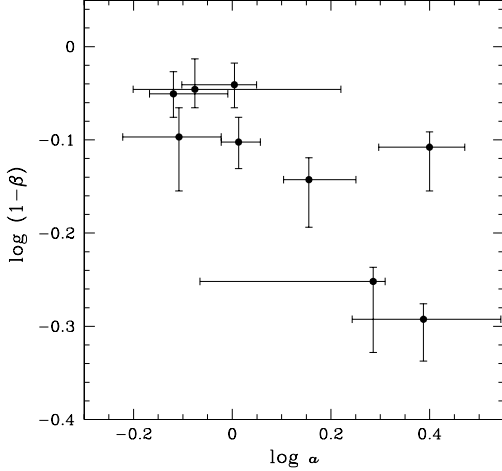


Figure 3. Relation between the halo parameters, (a is in units of R_{opt})

where I_n and K_n are the modified Bessel functions, V_{opt} is the measured circular velocity at R_{opt} and $\beta \equiv \left(\frac{V_D^2}{V^2}\right)_{R_{opt}}$.

The parameter β represents the disk contribution to the total circular velocity at R_{opt} and can vary from 0 to 1. On grounds of simplicity, we choose β as the disk free parameter rather than the disk mass-to-light ratio.

For the DM halo we assume a spherical distribution, whose contribution to the circular velocity $V_H(r)$ is given by (Persic, Salucci & Stel 1996, Salucci 1997):

$$V_H^2(r) = V_{opt}^2 \gamma (1 + a^2) \frac{x^2}{(x^2 + a^2)} \quad (4)$$

where $x \equiv r/R_{opt}$ and a is the core radius measured in units of R_{opt} . From eq.(1): $\gamma = (1 - \beta)$. Since we normalize (at R_{opt}) the velocity model $(V_H^2 + V_D^2)^{1/2}$ to the observed rotation speed V_{opt} , β enters explicitly in the halo velocity model and this reduces the free parameters of the mass model to two.

It is important to remark that, out to R_{opt} , the proposed Constant Density Region (CDR) model of eq.(4) is neutral with respect to the competing mass models. Indeed, by varying β and a , it approximately reproduces the maximum-disk, the solid-body, the no-halo, the all-halo, the CDM and the coreless-halo models. For instance, CDM halos with concentration parameter $c = 5$ and $r_s = R_{opt}$ (see §5) are well fit by eq.(4) with $a \simeq 0.33$.

For each galaxy, we determine the values of the parameters β and a by means of a χ^2 -minimization fit to the observed rotation curves:

$$V_{model}^2(r; \beta, a) = V_D^2(r; \beta) + V_H^2(r; \beta, a) \quad (5)$$

A central role in discriminating among the different mass decompositions is played by the derivative of the velocity field dV/dr . It has been shown (e.g. Persic & Salucci 1990b, Persic & Salucci 1992) that by taking into account the logarithmic gradient of the circular velocity field defined as:

$$\nabla(r) \equiv \frac{d \log V(r)}{d \log r} \quad (6)$$

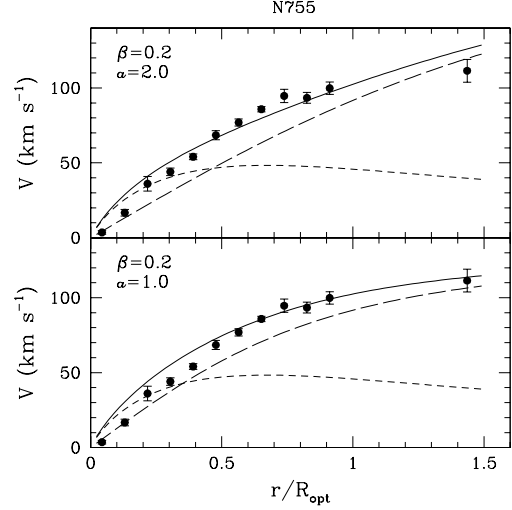


Figure 4. N755 rotation curve compared with over-maximum-disk models ($\beta = 0.2$ and $a = 2.0$ (top) or $a = 1.0$ (bottom)). Solid line represents the total circular velocity, short- and long-dashed lines represent the disk and halo contributions. The best-fit model for this galaxy has $\beta = 0.09^{+0.05}_{-0.05}$ and $a = 1.0^{+0.1}_{-0.2}$, corresponding to $M_D/L_I = 0.2 M_\odot/L_{I \odot}$. We realize that models with significantly higher disk mass-to-light ratio are inconsistent with the inner rotation curve, regardless of the halo profile.

one can significantly increase the amount of information available from kinematics and stored in the shape of the rotation curve. So we consider χ^2 -s calculated on both velocities and logarithmic gradients:

$$\chi_V^2 = \sum_{i=1}^{n_V} \frac{V_i - V_{model}(r_i; \beta, a)}{\delta V_i} \quad (7)$$

$$\chi_\nabla^2 = \sum_{i=1}^{n_\nabla} \frac{\nabla(r_i) - \nabla_{model}(r_i; \beta, a)}{\delta \nabla_i} \quad (8)$$

where $\nabla_{model}(r_i, \beta, a)$ is computed from eq.(3)–(4) and eq.(6). As the linear combination of χ^2 -s still follows the χ^2 -statistics (Bevington & Robinson 1992), we derived the parameters of the mass models by minimizing a total χ_{tot}^2 , defined as:

$$\chi_{tot}^2 \equiv \chi_V^2 + \chi_\nabla^2 \quad (9)$$

The above is the $\alpha = 1$ case of the general relation $\chi_{tot}^2 \equiv \chi_V^2 + \alpha \cdot \chi_\nabla^2$ we adopt in that the circular velocity at radius r_i and the corresponding log-gradient $\nabla(r_i)$ are statistically independent. Notice that the χ_{tot}^2 best-fit solutions are not statistically different from those obtained with the usual χ^2 procedure, however, the ellipse uncertainty is now remarkably reduced.

The parameters of the best-fit models are listed in Table 2, along with their 1σ uncertainties. The mass models are well specified for each object: the allowed values for β and a span a small and continuous region of the (a, β) space. We get a “lowest” and a “highest” halo velocity curve by subtracting from $V(r)$ the maximum and the minimum disk contributions $V_D(r)$ obtained by substituting in eq.(3) the parameter β with $\beta_{best} + \delta\beta$ and $\beta_{best} - \delta\beta$, respectively.

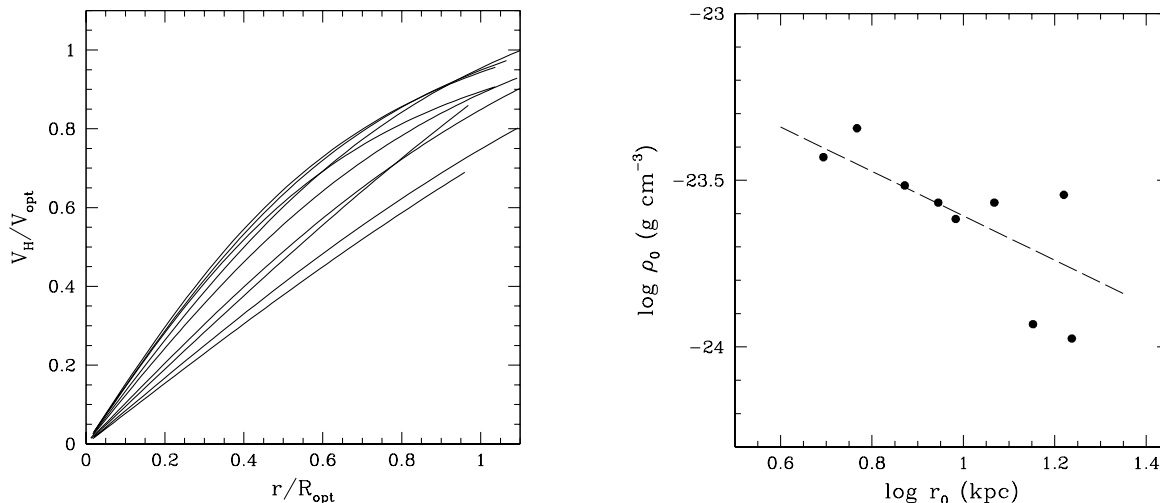


Figure 5. (*left*): The halo velocity profiles of the sample galaxies. $V_H(r)$ rises almost linearly with radius: the DM halo density remains approximately constant (*right*): halo central density ρ_0 vs. core radius r_0 . The dashed line is the Burkert relationship for dwarf galaxies.

The derived mass models are shown in Figure 2, alongside with the separate disk and halo contributions. It is then obvious that the halo curve is steadily increasing, almost linearly, out to the last data point. The disk-contribution β and the halo core radius a span a range from 0.1 to 0.5 and from 0.8 to 2.5, respectively. In each object the uniqueness of the resulting halo velocity model can be realized by the fact that the maximum-disk and minimum-disk models almost coincide. In Figure 3 we show the correlation between the halo parameters: halos which are more dynamically important at R_{opt} (i.e. with higher $1 - \beta$) have smaller core radii. Part of the scatter of the relation may arise because the sample is limited in statistics and in luminosity range (see Salucci and Burkert, 1999). Remarkably, we find that the size of the halo density core is always greater than the disk characteristic scale-length R_D and it can extend beyond the disk edge (and the region investigated).

As regards to the HI disk contribution, we checked the consequence of neglecting it. Its contribution to the circular velocity (see §3, Corbelli and Salucci, 1999) is computed and then actually subtracted from $V(r)$. As result, the values of the parameter β do not change whereas we obtain slightly larger values of the core radius a . As a typical example: for N755, considering the gas distribution we get: $\beta = 0.05^{+0.07}_{-0.05}$ and $a = 1.1^{+0.2}_{-0.2}$ to be compared with the value in Table 2.

Although the present sample is small for a thorough investigation of the stellar mass-to-light ratios, it is worth noticing that the disk mass-to-light ratios found ($< M_D/L_I > \sim 0.8 M_\odot/L_{I\odot}$) are typical of late-type spirals with young dominant stellar populations and ongoing star formation (e.g. de Jong, 1996), which adds to variations in stellar populations due to differences in age, metallicity, star formation history and to uncertainties in the estimate of distances and/or internal extinctions. In detail, we ensured that for the three galaxies with the lowest disk mass-to-light ratios, a significantly larger value of β was inconsistent with the (inner) rotation curve (see Figure 4).

Finally, it is worth stressing that the present analysis computes the mass-to-light ratio from the model parameters as a secondary quantity; the uncertainties in Col.(4) of Table 2 do not indicate the goodness of the *halo* mass models, but only specify how well we know this quantity.

4 DARK HALOS PROPERTIES

In Figure 5 (*left*) we show the halo velocity profiles for the nine galaxies. The halo circular velocities are normalized to their values at R_{opt} and expressed as a function of the normalized radius r/R_{opt} . These normalizations allow a meaningful comparison between halos of different masses: the radius scaling removes the intrinsic dependence of size on mass (more massive halos are bigger), whereas the velocity scaling takes into account that more luminous galaxies have higher circular velocities. It is then evident that the halo circular velocity, in every galaxy, rises almost linearly with radius, at least out to the disk edge:

$$V_H(r) \propto r \quad 0.05 R_{opt} \lesssim r \lesssim R_{opt} \quad (10)$$

The halo density profile has a well defined core radius within which the density is approximately constant. This is inconsistent with the singular halo density distribution emerging in the Cold Dark Matter (CDM) scenario of halo formation (Navarro, Frenk & White (NFW) 1995, 1996, 1997; Cole & Lacey, 1997; Tormen et al., 1997; Tissera & Dominguez-Tenreiro, 1998; Nusser & Sheth, 1999). More precisely, since the CDM halos are, at small radii, likely more cuspy than the NFW profile: $\rho_{CDM} \propto r^{-1.5}$ (Fukushige & Makino, 1997; Moore et al., 1998; Jing, 1999; Jing & Suto, 1999; Ghigna et al., 1999), the steepest CDM halo velocity profile $V_H(r) \propto r^{1/4}$ results too shallow with respect to observations and therefore inconsistent with eq.(10). Burkert (1995) has proposed for the halo density distribution the following phenomenological profile:

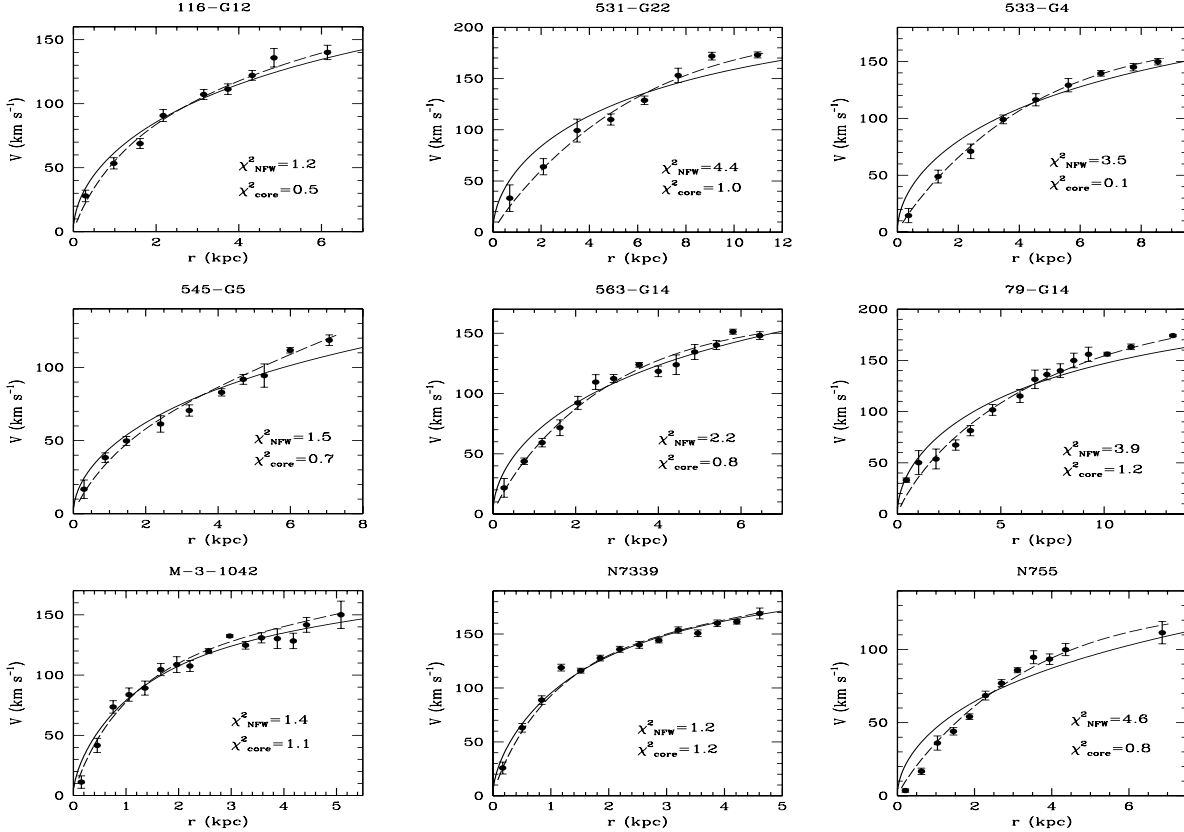


Figure 6. NFW best-fits *solid lines* of the rotation curves (*filled circles*) compared with the CDR fits (*dashed lines*). The χ^2 values are also indicated.

$$\rho_B(r) = \frac{\rho_0 r_0^3}{(r + r_0)(r^2 + r_0^2)} \quad (11)$$

where ρ_0 (the central density) and r_0 (the scale radius) are free parameters. This density law has a core radius of size r_0 , and, at large radii, converges to the NFW profile. The two parameters ρ_0 and r_0 are found correlated: $\rho_0 \sim r_0^{-2/3}$, so that the halo profiles reduce to a one-parameter family of curves (Burkert, 1995).

We find that, by adjusting ρ_0 and r_0 , we can reproduce, over the available radial range, the halo velocity profiles of eq.(4) and Table 1. We show in Figure 5 (*right*) the pairs (ρ_0, r_0) corresponding to the 9 objects. The typical uncertainties on ρ_0 and r_0 are estimated at a level of about 0.15 dex and 0.07 dex, respectively: we then confirm the structure relation Burkert (1995) found for 5 dwarf galaxies (see Figure 5 *right*).

Let us stress that the CDR halo properties of eq.(10) raise important issues by themselves and make quite irrelevant, in comparing theory and observations, arguments *per se* important such as the CDM halos cosmic variance, the actual value of the concentration parameter or the effects of baryonic infalls or outflows (e.g. Martin, 1999; Gelato & Sommer-Larsen, 1999).

We also want to remark that our finding implies that disk galaxies are embedded (inside R_{opt}) in a *single* dark halo. Indeed, if more dark halos were relevantly present,

then, in order to not violate the constraint given by eq.(10), all of them should have the same solid body velocity profile.

5 THE INADEQUACY OF CDM MASS MODELS

Although the mass models of eq.(4) converge to a distribution with an inner core rather than with a central spike, i.e. to $a \simeq 1$ rather than to $a \simeq 1/3$, it is worth, given the importance of such result, to also check in a direct way the (in)compatibility of the CDM models with the observed kinematics. We assume the two-parameters functional form for the halo density by Navarro, Frenk & White (NFW, 1995, 1996, 1997):

$$\rho_{\text{NFW}}(r) = \frac{\rho_s}{(r/r_s)(1 + r/r_s)^2} \quad (12)$$

where r_s is a characteristic inner radius and ρ_s the corresponding density. In order to translate the density profile into a circular velocity curve for the halo, we make use of virial parameters: the halo virial radius R_{vir} , defined as the radius within which the mean density is Δ_{vir} times the mean universal density ρ_m at that redshift, and the associated virial mass M_{vir} and velocity $V_{\text{vir}} \equiv GM_{\text{vir}}/R_{\text{vir}}$. By defining the concentration parameter as $c_{\text{vir}} \equiv R_{\text{vir}}/r_s$ the

Galaxy	$M_{\text{vir}} \leq 2 \cdot 10^{12} M_{\odot}$				No limit on M_{vir}			
	β	c_{vir}	r_s (kpc)	M_D/L_I	β	c_{vir}	r_s (kpc)	$\log(M_{\text{vir}}/M_{\odot})$
116-G12	0.01 ^{+0.04} _{-0.01}	7.9 ^{+0.6} _{-0.4}	26 ⁺⁴ ₋₅	0.04 ^{+0.14} _{-0.04}	0.01 ^{+0.04} _{-0.01}	2.0 ^{+1.6} _{-0.2}	456 ⁺⁵⁰ ₋₁₀₀	14.3 ^{+0.3} _{-0.3}
531-G22	0.01 ^{+0.03} _{-0.01}	7.5 ^{+0.5} _{-0.5}	28 ⁺⁴ ₋₃	0.03 ^{+0.10} _{-0.03}	0.01 ^{+0.01} _{-0.01}	1.8 ^{+0.8} _{-0.1}	472 ⁺²⁰ ₋₉₀	14.0 ^{+0.2} _{-0.2}
533-G4	0.01 ^{+0.03} _{-0.01}	7.0 ^{+0.5} _{-0.5}	30 ⁺⁵ ₋₄	0.04 ^{+0.11} _{-0.04}	0.01 ^{+0.03} _{-0.01}	1.7 ^{+0.9} _{-0.2}	500 ⁺²⁰ ₋₈₀	13.9 ^{+0.3} _{-0.3}
545-G5	0.01 ^{+0.04} _{-0.01}	4.7 ^{+0.3} _{-0.7}	44 ⁺⁵ ₋₄	0.03 ^{+0.12} _{-0.03}	0.01 ^{+0.02} _{-0.01}	1.4 ^{+0.7} _{-0.1}	479 ⁺³⁰ ₋₉₀	13.4 ^{+0.2} _{-0.3}
563-G14	0.01 ^{+0.03} _{-0.01}	8.7 ^{+0.3} _{-0.7}	24 ⁺⁴ ₋₄	0.03 ^{+0.10} _{-0.03}	0.05 ^{+0.05} _{-0.05}	2.0 ^{+1.6} _{-0.2}	472 ⁺³⁰ ₋₇₀	14.3 ^{+0.2} _{-0.3}
79-G14	0.01 ^{+0.04} _{-0.01}	6.5 ^{+0.5} _{-0.5}	32 ⁺³ ₋₄	0.03 ^{+0.14} _{-0.03}	0.01 ^{+0.02} _{-0.01}	1.6 ^{+0.4} _{-0.2}	490 ⁺²⁰ ₋₁₁₀	13.8 ^{+0.2} _{-0.3}
M-3-1042	0.20 ^{+0.05} _{-0.10}	8.1 ^{+1.4} _{-0.6}	26 ⁺³ ₋₇	0.72 ^{+0.18} _{-0.36}	0.31 ^{+0.05} _{-0.06}	1.7 ^{+1.3} _{-0.2}	493 ⁺³⁰ ₋₁₂₀	14.0 ^{+0.3} _{-0.5}
N7339	0.18 ^{+0.02} _{-0.08}	11.1 ^{+2.0} _{-0.6}	19 ⁺² ₋₄	0.58 ^{+0.06} _{-0.26}	0.38 ^{+0.04} _{-0.08}	1.9 ^{+1.6} _{-0.3}	497 ⁺²⁰ ₋₈₀	14.2 ^{+0.3} _{-0.4}
N755	0.03 ^{+0.02} _{-0.03}	4.8 ^{+0.2} _{-0.8}	43 ⁺³ ₋₄	0.05 ^{+0.04} _{-0.05}	0.01 ^{+0.02} _{-0.01}	1.5 ^{+0.9} _{-0.2}	467 ⁺³⁰ ₋₁₁₀	13.6 ^{+0.1} _{-0.3}

Table 3. NFW mass models: (1) Galaxy name; (2)-(3)-(4)-(5) Parameters of the NFW best-fit models with their 1σ uncertainties. An upper limit of $2 \cdot 10^{12} M_{\odot}$ is imposed on M_{vir} . Disk mass-to-light ratios in the I -band in Col.(5) are in solar units; (6)-(7)-(8)-(9) Parameters of the best-fit models with no constraint on the virial mass.

halo circular velocity $V_{\text{CDM}}(r)$ takes the form (Bullock et al. 1999):

$$V_{\text{CDM}}^2(r) = V_{\text{vir}}^2 \frac{c_{\text{vir}}}{A(c_{\text{vir}})} \frac{A(x)}{x} \quad (13)$$

where $x \equiv r/r_s$ and $A(x) \equiv \ln(1+x) - \frac{x}{1+x}$. As the relation between V_{vir} and R_{vir} is fully specified by the background cosmology, we assume the currently popular Λ CDM cosmological model, with $\Omega_m = 0.3$, $\Omega_{\Lambda} = 0.7$ and $h = 0.75$, in order to reduce from three to two (c_{vir} and r_s) the independent parameters characterizing the model. According to this model, $\Delta_{\text{vir}} \simeq 340$ at $z \simeq 0$. The choice is conservative: a high density $\Omega_m = 1$ model, with a concentration parameter $c_{\text{vir}} > 12$, is definitely unable to account for the observed galaxy kinematics (Moore 1994).

Though N-body simulations and semi-analytic investigations indicate that the two parameters c_{vir} and r_s seem to correlate, we leave them independent to increase the chance of a good fit. Since the objects in our sample are of low luminosity, i.e. $L_*/12 \lesssim L_I \lesssim L_*/3$, we conservatively set for the halo mass M_{vir} an upper limit of $M_{\text{up}} = 2 \times 10^{12} M_{\odot}$, comparable to the total mass of the Galaxy (e.g. Wilkinson & Evans, 1999) and to the mass of bright spirals in pairs (e.g. Chengalur, Salpeter & Terzian, 1993). This value is further justified by considering that, if $M_{\text{vir}} > M_{\text{up}}$ in the above-specified luminosity range, then, the amount of dark matter locked in spiral galaxies $\Omega_S = \int_{L_*/12}^{L_*/3} M_{\text{vir}} \phi(L) dL$, with $\phi(L)$ the galaxy luminosity function, would much exceed 0.1, and would be unacceptable for the assumed cosmological model having $\Omega_m = 0.3$.

We performed the fit to the data with the χ_{tot}^2 minimization technique described in §3; the results are reported in Table 3, Col.(1)...(5). In Figure 6 we compare the CDR and the NFW models: for 7 galaxies the NFW model is unacceptably worse than the CDR solution, whereas for 2 objects (M-3-1042 and N7339) the goodness level of the two different fits is comparable, but the virial mass in the case of CDM is quite high: $M_{\text{vir}} \sim 2 \times 10^{12} M_{\odot}$. Moreover, the CDM models have extremely low value for the disk mass-to-light ratio (see Table 3 Col.5). The majority of the objects have $M_D/L_I \leq 0.05$, in obvious disagreement with

the spectro-photometric properties of spirals, that indicate mass-to-light ratios at least 10 times higher.

The inadequacy of the CDM model for our sample galaxies is even more evident if one performs the fit after removing any constraint on virial mass. Indeed, (results in Table 3, from Col.6 to 9), good fits are obtained only for very low values of the concentration parameter ($c_{\text{vir}} \simeq 2$) and for uncomfortably large virial velocities and masses ($V_{\text{vir}} \simeq 600 - 800 \text{ km s}^{-1}$; $M_{\text{vir}} \simeq 10^{13} - 10^{14} M_{\odot}$). These results can be explained as effect of the attempt of the minimization routine to fit the $V(r) \propto r^{0.5}$ NFW velocity profile to data intrinsically linear in r .

6 SUMMARY AND CONCLUSIONS

We have performed the disk-halo decomposition for a well suited sample of 9 bulge-less disk galaxies with $100 \leq V_{\text{opt}} \leq 170 \text{ km s}^{-1}$. These galaxies have a relevant amount of dark matter: the contribution of the luminous matter to the dynamics is small and it can be properly taken into account. Moreover, the high spatial resolution of the available rotation curves allows us to obtain the separate dark and luminous density profiles. We find that dark matter halos have a constant central density region whose size exceeds the stellar disk length-scale R_D . These halo profiles disagree with the cuspy density distributions typical of CDM halos (e.g. Navarro, Frenk & White, 1997; Kravtsov et al., 1998), which, therefore, fail to account for the actual DM velocity data. On the other hand, these halo velocities are well described in terms of the Burkert density profile, an empirical functional form whose two structure parameters (central density and core radius) are related through: $\rho_0 \sim r_0^{-2/3}$.

This work is complementary to that of Salucci (2000) who derived for 140 objects of different luminosity ∇_h , the logarithmic gradient of the halo velocity slope at R_{opt} . Reminding that $\nabla_h = 0$ and $\nabla_h = 1$ mean an isothermal and a solid-body regime, respectively, let us stress that the result found: $\nabla_h \leq 1$ completely supports, at the optical edge, the results of the present paper obtained for a small sample of spirals over the entire stellar disk.

Finally, the dark halo velocity linear rise from $0.25R_D$ to

$\sim 3R_D$ sets a serious upper limit to the dynamical relevance of CDM-like dark halos in spirals. Indeed, once we rule out a CDM halo, also the claim by Burkert and Silk (1997) of *two* dark halos, a MACHO dark halo with a CDR profile and a standard CDM halo, meets a difficulty. Indeed, in this case, in order to satisfy eq.(10), the MACHO halo should account for $> 95\%$ of the dark mass inside R_{opt} . Then, it would dominate the dynamics out to well beyond $25 R_D$. The CDM halo would then have dynamical importance in regions so external that its cosmological role itself would be in question.

REFERENCES

- Begeman, K.G., Broeils, A.H. & Sanders, R.H. (1991) MNRAS, **249**, 523.
- Bevington, P.R. & Robinson, D.K. (1992) *Data reduction and error analysis*; Boston: McGraw-Hill
- Blais-Ouellette, S., Carignan, C., Amram, P. & Coté, S. (1999) astro-ph/9911223.
- Bullock, J.S., Kolatt, T.S., Sigad, Y., Somerville, R.S., Kravtsov, A.V., Klypin, A.A., Primack, J.R. & Dekel, A. (1999) astro-ph/9908159.
- Burkert, A. (1995) ApJ, **447**, L25.
- Burkert, A. & Silk, J. (1997) ApJ, **488**, L55.
- Chengalur, J.N., Salpeter, E.E. & Terzian, Y. (1993) ApJ, **419**, 30C.
- Cole, S. & Lacey, C. (1997) MNRAS, **281**, 716.
- Corbelli, E. & Salucci, P. (1999) astro-ph/9909252
- Coté, S. & Carignan, C. (1991) AJ, **102**, 904.
- de Jong, R.S. (1996) A&A, **313**, 377.
- Flores, R. & Primack, J.R. (1994) ApJ, **427**, L1.
- Freeman, K.C., (1970) ApJ, **160**, 811F.
- Fukushige, T. & Makino, J. (1997) ApJ, **477**, L9.
- Gelato, S. & Sommer-Larsen, J. (1999) MNRAS, **303**, 321.
- Ghigna, S., Moore, B., Governato, F., Lake, G., Quinn, T. & Stadel, J. (1999) preprint (astro-ph/9910166)
- Jing, Y.P., (1999) ApJ, **515L**, 45J
- Jing, Y.P. & Suto, Y. (1999) in press, (astro-ph/9909478)
- Kravtsov, A.V., Klypin, A.A., Bullock, J.S., & Primack, J.R. (1998) ApJ, **502**, 48.
- Martin, C.L. (1999) ApJ, **513**, 142.
- Mathewson, D.S., Ford, V.L. & Buchhorn, M.K.C. (1992) ApJS, **81**, 413.
- McGaugh, S.S., & de Block, W.J.G. (1998) ApJ, **499**, 41.
- Moore, B. (1994) Nature, **370**, 629.
- Moore, B., Governato, F., Quinn, T., Stadel, J., & Lake, G. (1998) ApJ, **499**, L5.
- Navarro, J.F., Frenk, C.S. & White, S.D.M. (1995) MNRAS, **275**, 56.
- Navarro, J.F., Frenk, C.S. & White, S.D.M. (1996) ApJ, **462**, 563.
- Navarro, J.F., Frenk, C.S. & White, S.D.M. (1997) ApJ, **490**, 493.
- Nusser, A. & Sheth, R.K. (1999) MNRAS, **303**, 685N.
- Persic, M. & Salucci, P. (1990b) MNRAS, **245**, 577
- Persic, M. & Salucci, P. (1992) Astro. Lett. and Communications, **28**, 307
- Persic, M. & Salucci, P. (1995) ApJS, **99**, 501 (PS95)
- Persic, M., Salucci, P. & Stel, F. (1996) MNRAS, **281**, 27P
- Puche, D., Carignan, C. & Bosma, A. (1990) AJ, **100**, 1468
- Rhee, M.-H. (1996) PhD thesis, Groningen University
- Salucci, P. (1997) ASP Conference Series, **117**
- Salucci, P. (1999) MNRAS accepted
- Salucci, P., Ratnam, C., Monaco P., Danese, L., (1999) MNRAS in press, (astro-ph/9812485)
- Salucci, P. & Burkert, A. (1999) ApJ in press
- Salucci, P. & Persic, M. (1995) Mem.S.A.It., **Vol.66**^o, 1
- Salucci, P. & Persic, M. (1999a) MNRAS, **309**, 923
- Stil, J. (1999) Ph.D. Thesis, Leiden University
- Tissera, P.B. & Dominguez-Tenreiro, R. (1998) MNRAS, **297**, 177
- Tormen, G., Bouchet, F.R. & White, S.D.M. (1997) MNRAS, **286**, 865
- van Albada, T.S., Bahcall, J.S., Begeman, K. & Sancisi, R. (1985) ApJ, **295**, 305
- van den Bosch, F.C., Robertson, B.E., Dalcanton, J. & de Blok, W.J.G. (1999) astro-ph/9911372
- Verheijen, M.A.W. (1997), Ph.D. Thesis (Cap. 6), Groningen University
- Wilkinson, M.I. & Evans, N.W. (1999) MNRAS, **310**, 645